Microelectronic Engineering 106 (2013) 164–167

Contents lists available at SciVerse ScienceDirect

Microelectronic Engineering

journal homepage: www.elsevier.com/locate/mee

Highly adhesive electroless barrier/Cu-seed formation for high aspect ratio through-Si vias

Fumihiro Inoue [a], Tomohiro Shimizu [a], Hiroshi Miyake [a], Ryohei Arima [a], Toshihiko Ito [b], Hirofumi Seki [b], Yuko Shinozaki [b], Tomohiko Yamamoto [b], Shoso Shingubara [a,*]

[a] Kansai University, 3-3-35 Yamate, Suita, Osaka, Japan
[b] Toray Research Center. Inc., 3-3-7 Sonoyama, Otsu, Shiga, Japan

ARTICLE INFO

Article history:
Available online 11 January 2013

Keywords:
Through Si via
Diffusion barrier layer
Seed layer
Electroless plating
Pd nano particles

ABSTRACT

A conformal diffusion barrier was formed in a high aspect ratio through-silicon via using electroless plating. Dense adsorption of Pd nanoparticle catalyst on SiO_2 assisted the formation of a thin electroless Co–W–B layer, upon which an electroless Cu seed layer could be deposited. The adhesion strength of the Co–W–B film was enhanced by reducing the film thickness, and the maximum strength was obtained at a thickness of 20 nm. The Co–W–B layer exhibited good barrier properties against Cu diffusion to SiO_2 after annealing at 300 °C, although slight diffusion of the Pd atoms in Cu was observed.

1. Introduction

Three-dimensional (3D) integration technology for high packaging density has recently attracted considerable attention. The filling of metal in through-Si via (TSV) has been extensively studied as a key technology for 3D integration [1]. TSV is also a potential candidate for the substitute of global interconnections in ultra-large-scale integrated circuits (ULSIs) in the near future. In such a structure, the TSV diameter is expected to be less than 2 μm, and the aspect ratio larger than 10 [2]. Copper is the most appropriate filling metal for a TSV, because of its low resistivity. In addition, copper can be applied using electrodeposition, which would result in cost reduction, and good filling property for a high aspect ratio structure. There have been many studies using Cu electrodeposition that have achieved void-free TSV filling [3–7]; however, most of these studies have utilized high-cost processes in the formation of the barrier and seed layers prior to Cu electrodeposition. Cost reduction of the barrier and seed layer deposition processes is a main challenge for the practical application of Cu-TSVs. Furthermore, for the via-last Cu-filling process, which is a TSV process conducted after the back end of line interconnect, a reduction of the process temperature is required to improve device reliability. Nevertheless, conventional methods for the formation of barrier and seed layers, such as chemical vapor deposition (CVD) or physical vapor deposition (PVD), both require expensive high-vacuum systems. Furthermore, a PVD sputtered layer reaches the limits for the formation of a continuous layer at the bottom of the TSV due to low step coverage. CVD-TiN or W can be used to form a reliable barrier layer, even in a high aspect ratio structure; however, it requires a high temperature processing over 400 °C.

Recently, Ni and Co alloys deposited by electroless deposition have attracted considerable attention as alternative barrier metals, due to their low processing temperature and good thermal stability against Cu diffusion [8,9]. Moreover, selective deposition of the capping metal, such as Co–W–B and Co–W–P, on the Cu interconnection to improve the resistance to electromigration has been investigated [10–12]. We have previously achieved the successful formation of both barrier and seed layers by electroless deposition with Au nanoparticles (Au-NPs) as a catalyst [13]. However, the use of Au in a Si process may cause serious metal contamination issues. In this work, we investigated an electroless deposition of Co-W-B and Cu as barrier/seed layers using Pd nanoparticles (Pd-NPs) as an alternative catalyst to Au-NPs. In addition, the adhesion strength between the barrier films and SiO_2, and the resistance of the electroless Co–W–B layer against Cu diffusion were evaluated.

2. Experimentals

The TSVs were 2 μm in diameter and 24 μm deep. A 200-nm-thick dielectric SiO_2 layer was formed by thermal oxidation. The SiO_2 surface was immersed in a solution of 3-aminopropyltriethoxysilane with toluene as a solvent at 60 °C for 1 h, prior to electroless Co–W–B deposition [14]. After the formation of organosilane monolayer, 4-nm-diameter Pd-NPs (Tanaka Precious

* Corresponding author. Address: Department of Mechanical Engineering, Kansai University, 3-3-35 Yamate-Cho, Suita, Osaka, Japan. Tel./fax: +81 6 6368 0881.
E-mail address: shingu@kansai-u.ac.jp (S. Shingubara).

0167-9317/$ - see front matter © 2013 Elsevier B.V. All rights reserved.
http://dx.doi.org/10.1016/j.mee.2013.01.009

Metals Co. Ltd.) were adsorbed on the SiO_2 surface at room temperature. The Pd-NPs were stabilized in pure water using polyvinylpyrrolidone (PVP) as a dispersant. Electroless Co–W–B deposition as a barrier layer was then conducted using the adsorbed Pd-NP catalyst. The electroless Co–W–B plating solution contained 0.17 mol/L of cobalt sulfate, 0.005 mol/L of tungsten acid, 0.049 mol/L of dimethylamine borane (DMAB) as a reducing agent, and 0.63 mol/L of citric acid as a complexing agent [8–13]. In addition, bis(3-sulfopropyl) disulfide (SPS) was added to control the deposition profile for the high aspect ratio TSV. The pH was 9.5 and the plating temperature was 60 °C. An electroless Cu layer was deposited directly on the Co–W–B layer by displacement plating at 70 °C. In addition, SPS and chloride ions were added as inhibitors. The details of chemicals used in the electroless Cu bath are described in Refs. [15–17]. The adhesion strengths were measured using the stud pull test (Romulus, Quad Group Inc.). Cross-sectional views of the TSVs were obtained by field emission scanning electron microscopy (FE-SEM; Jeol JSF-7500F) and field emission transmission electron microscopy (FE-TEM; Jeol JEM-2100F). Elemental depth profiles were obtained by secondary ion mass spectrometry (SIMS; PHI ADEPT-1010) analysis from the backside of the Si substrate.

3. Results and discussion

The electroless plating of the Co–W–B barrier layer did not occur directly on the dielectric layer. Therefore, sufficient nucleation sites, such as the Pd-NP catalyst, were necessary for the formation of the electroless barrier layer. Catalyst adsorption for electroless deposition is generally conducted using PdCl solution and/or Sn/Pd colloids [18]. However, Sn/Pd colloids tend to agglomerate at the top of the TSV, which makes it difficult to control the catalyst size [8,18]. To adsorb high-density catalyst particles throughout a high aspect ratio TSV, a self-assembled monolayer (SAM) and Pd-NPs were used on the SiO_2 dielectric layer. The Pd-NPs were dispersed in a solution, which enabled adsorption on the surface with high density and without agglomeration.

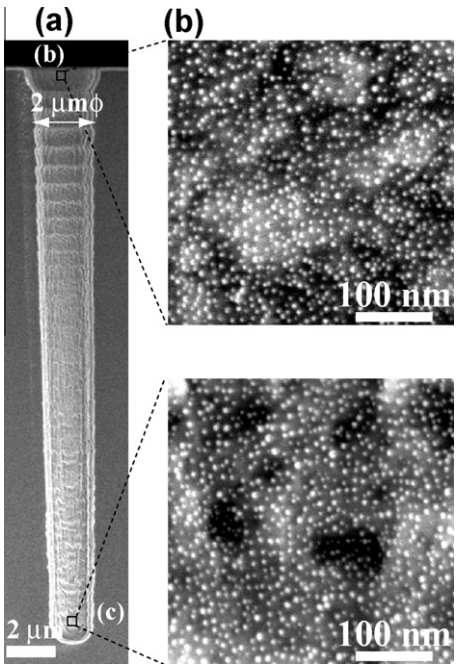

Fig. 1. Cross-sectional SEM images after adsorption of Pd-NPs on the TSV sidewall. (a) Overview, (b) top, and (c) bottom of the TSV.

Fig. 1 shows cross-sectional SEM images of different parts of a TSV after the adsorption of Pd-NPs for 3 h. A high density of Pd-NPs was observed throughout the entire TSV, and there was no evidence of Pd-NP agglomeration. This was probably due to the use of PVP to disperse the Pd-NPs. The PVP molecules remained on the surface of the Pd-NPs even after adsorption onto the SiO_2, and the negative charge of the PVP generated a repulsive force between the Pd-NPs [19].

Fig. 2 shows cross-sectional TEM images of an electroless Cu/Co–W–B plated TSV. Electroless Co–W–B plating was performed in the TSV using Pd-NPs as a catalyst. A continuous and uniform Co–W–B film with a thickness of 60 nm was deposited throughout the TSV. The thickness of the Co–W–B film was relatively uniform, even though there was a periodic roughness of the TSV sidewall due to scalloping. The Co–W–B film had a fine polycrystalline grain structure with an average grain size of less than 5 nm, and the Cu film had a polycrystalline structure with a grain size larger than 50 nm. The Co–W–B film was composed of Co with 15% W, according to TEM-EDX analysis.

After formation of the Co–W–B layer, electroless Cu plating was performed to form a seed layer. Electroless Cu can be directly deposited on several barrier metals by displacement plating [20]. SPS (0.1 ppm) and Cl^- (5 ppm) were added as inhibitors to realize a bottom-up filling tendency by electroless Cu plating, as shown in the TEM images of Fig. 2. The Cu thickness increased from the bottom to the top and no voids were evident near the bottom of the TSV. One of the authors (S. Shingubara) previously reported the bottom-up filling of electroless Cu in submicron holes assisted by the addition of inhibitor molecules [15]. These inhibitor molecules are tightly adsorbed on the Cu surface and suppress the reduction of Cu ions. Furthermore, some of the inhibitor molecules are included in the Cu film. The diffusion flux of inhibitors at the bottom of the hole was lower than that at the top; therefore, the film was thinner at the top of the TSV than at the bottom. The bottom-up

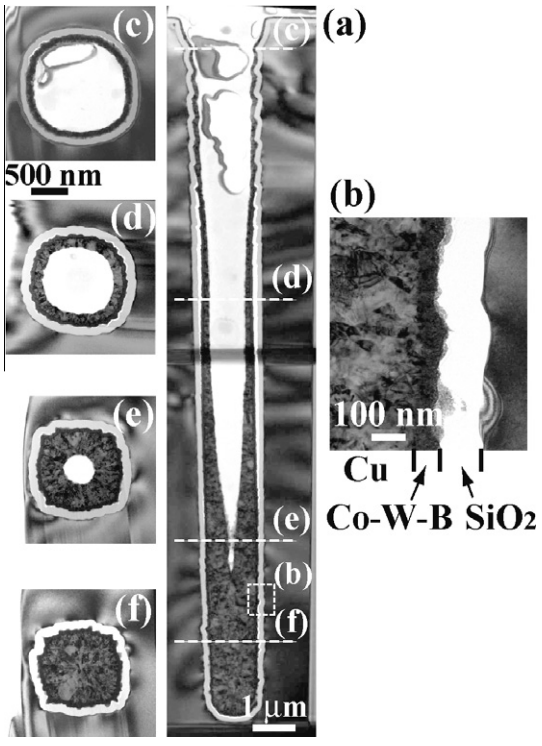

Fig. 2. TEM images of an electroless Cu/Co–W–B bilayer in a TSV. (a) Overview, (b) vertical cross-sectional image of sidewall, and (c–f) horizontal cross-sectional images at various depths.

filling by electroless Cu was observed only for TSVs with both a high aspect ratio and a fine circular well structure (2 μm diameter). The method of bottom-up filling by electroless Cu presented here would be a significant contribution to Cu filling electroplating processes, especially for high aspect TSVs.

Adhesion strength is an important factor in the reliability of 3-D integration technology. The adhesion strength between SiO_2 and electroless Co–W–B films was evaluated using a stud pull test. The samples on the SiO_2/Si substrate were bonded to a stud pin with epoxy resin at 150 °C for 1 h. In all cases, the data represents the average value of five identical sample tests. The adhesion strength of as-sputtered Co was 64 MPa and that of as-sputtered Ta was 86 MPa. The electroless Co-W–B film delaminated at its interface with SiO_2, and there were no Pd-NPs on the SiO_2 surface after delamination, which was confirmed with SEM observation and EDX analysis. Fig. 3(a) shows the dependence of adhesion strength on the film thickness. The adhesion strength was determined when film delamination occurred at the boundary between the film and the substrate during the pulling down of the stud. It is interesting that the adhesion strength increased linearly with decreasing film thickness. The adhesion strength was highest at 20 nm and the standard deviation of data was the lowest at this thickness. For film thicknesses less than 40 nm, the adhesion strength was as high as that of a sputtered Co film. The internal stress in the Co–W–B film increased with increasing film thickness. Delamination occurred when the internal stress surpassed the adhesion strength of the film. The detailed mechanism of the increase in internal stress is yet to be clarified, but the annihilation of atomic defects by grain growth during the growth of the film is probably an important factor. The segregation of B and other non-stoichiometric components could be another factor in the generation of internal stress. Fig. 3(b) shows the dependence of the adhesion strength on the annealing temperature for 80-nm-thick Co–W–B films annealed for 30 min in vacuum (1×10^{-4} Pa). The adhesion strength of the as-deposited Co–W–B film was 20 MPa; however, this was increased to 70 MPa after annealing at 200 °C. This marked increase in adhesion strength may be due to the relaxation of internal stress during annealing. After annealing at 300 °C, the film structure changed from amorphous to polycrystalline, according to XRD analysis. This change in the crystalline structure may have affected the adhesion strength of the film.

Fig. 4 shows depth profiles of the elements for the blanket Cu (65 nm)/Co–W–B (45 nm)/Pd-NPs/SiO_2 (300 nm)/Si substrate measured by backside-SIMS analysis. Cu, Pd and Co were not detected in the SiO_2 layer, even after annealing at 300 °C, which indicates that the electroless Co–W–B layer has good barrier properties against Cu diffusion. In addition, the distribution of Pd was slightly changed after annealing. Prior to annealing, a peak corresponding to Pd-NPs was observed at the interface between Co–W–B and SiO_2; however, the peak intensity decreased and the amount of Pd in the Cu layer increased after annealing, which suggests that Pd diffused toward the Cu layer during annealing.

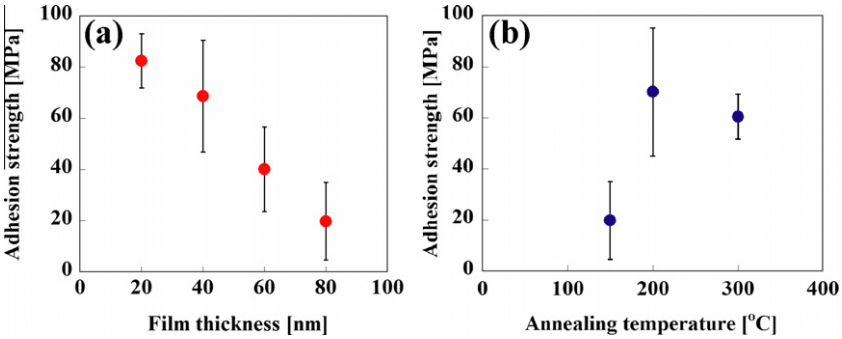

Fig. 3. Adhesion strength of the electroless Co–W–B layers. Dependence of adhesion strength on (a) film thickness and (b) annealing temperature.

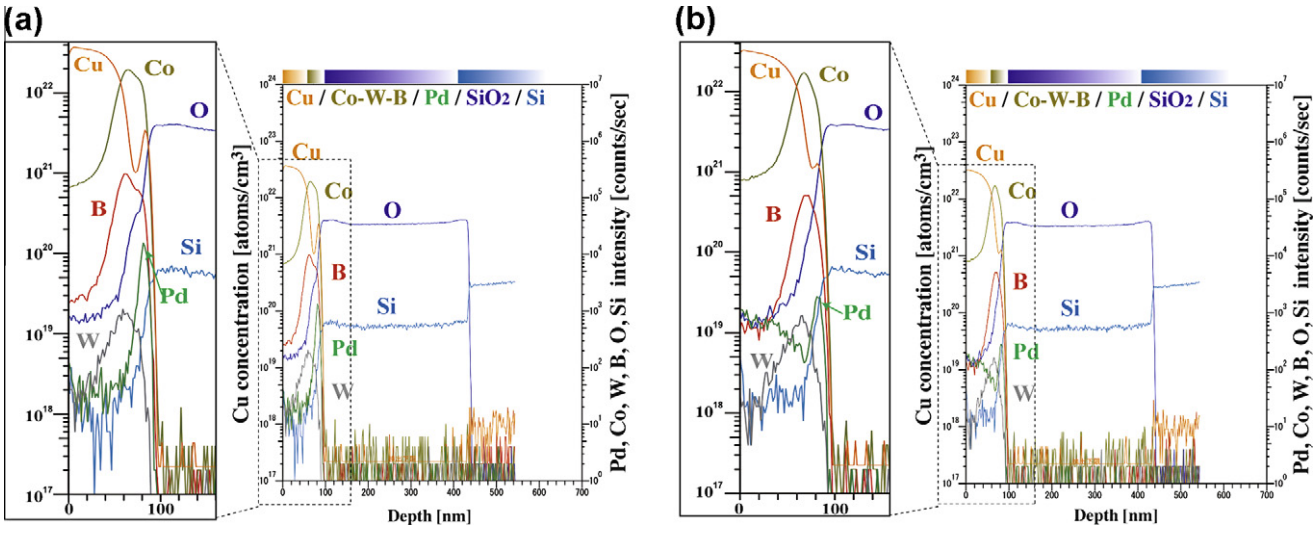

Fig. 4. Back-side SIMS depth profiles for Cu/Co–W–B/Pd-NPs/SiO_2/Si substrate.: (a) as-deposited and (b) after annealing at 300 °C for 30 min.

4. Conclusions

A thin continuous diffusion barrier was formed using electroless Co–W–B plating with a Pd-NP catalyst in fine TSV (2 μm diameter, AR 12). The high density adsorption of Pd-NPs assisted the efficient formation of a thin and continuous electroless Co–W–B layer. Moreover, an electroless Cu seed layer was deposited by a bottom-up mode. The adhesion strength of 40-nm-thick electroless Co–W–B films exceeded 80 MPa. The adhesion strength of the electroless Co–W–B films exceeded 70 MPa after annealing at 200 °C, even for a film thickness of 80 nm. In addition, the Co–W–B film has a good barrier properties against Cu diffusion, even after annealing at 300 °C. The proposed technology offers a low temperature and low cost diffusion barrier process for fine diameter and high aspect ratio TSVs.

Acknowledgements

This work was supported by the "Strategic Project to Support the Formation of Research Bases at Private Universities", a Matching Fund Subsidy from the Ministry of Education, Culture, Sports, Science and Technology (MEXT) of Japan. This work was also supported by a Research Fellowship from the Japan Society for the Promotion of Science (JSPS).

References

[1] E. Beyne, in Proceedings of the IEEE International Interconnect Technology Conference (IITC), IEEE, 2006 pp. 1.
[2] ITRS, Interconnects Roadmap, 2009, p. 8.
[3] J.J. Sun, K. Kondo, T. Okamura, S.J. Oh, M. Tomisaka, H. Yonemura, M. Hoshino, K. Takahashi, J. Electrochem. Soc. 150 (6) (2003) 596.
[4] K. Kondo, T. Yonezawa, D. Mikami, T. Okubo, Y. Taguchi, K. Takahashi, D.P. Barkey, J. Electrochem. Soc. 152 (11) (2005) H173.
[5] O. Lühn, A. Radisic, P.M. Vereecken, C. Van Hoof, W. Ruythooren, J.-P. Celis, Electrochem. Solid-State Lett. 12 (5) (2009) D39.
[6] O. Lühn, A. Radisic, C. Van Hoof, W. Ruythooren, J.-P. Celis, J. Electrochem. Soc. 157 (4) (2010) D242.
[7] C. Okoro, K. Vanstreels, R. Labie, O. Lühn, B. Vandevelde, B. Verlinden, D. Vandepitte, J. Micromech. Microeng. 20 (2010) 045032.
[8] A. Kohn, M. Eizenberg, Y. Shacham-Diamand, Y. Sverdlov, Mater. Sci. Eng. A 302 (2001) 18.
[9] T. Osaka, N. Takano, T. Kurokawa, K. Ueno, Electrochem. Solid-State Lett. 5 (2002) C7.
[10] Y. Shacham-Diamand, V. Dubin, M. Angyal, Thin Solid Films 262 (1995) 93.
[11] H. Nakano, T. Itabashi, H. Akahoshi, J. Electrochem. Soc. 152 (3) (2005) C163.
[12] J. Gambino, J. Wynne, J. Gill, S. Mongeon, D. Meatyard, B. Lee, H. Bamnolker, L. Hall, N. Li, M. Hernandez, P. Little, M. Hamed, I. Ivanov, C.L. Gan, Microelectron. Eng. 83 (2006) 2059.
[13] F. Inoue, T. Shimizu, T. Yokoyama, H. Miyake, K. Kondo, T. Saito, S. Tanaka, T. Terui, S. Shingubra, Electrochim. Acta 56 (6) (2011) 245.
[14] W.J. Dressick, C.D. Dukey, J.H. Georger Jr., G.S. Carabrese, J.M. Calvert, J. Electrochem. Soc. 141 (1) (1994) 210.
[15] S. Shingubara, Z. Wang, O. Yaegashi, R. Obata, H. Sakaue, T. Takahagi, Electrochem. Solid-State Lett. 7 (6) (2004) C78.
[16] F. Inoue, Y. Harada, M. Koyanagi, T. Fukushima, K. Yamamoto, S. Tanaka, Z. Wang, S. Shingubara, Electrochem. Solid-State Lett. 12 (10) (2009) H381.
[17] F. Inoue, H. Philipsen, A. Radisic, S. Armini, Y. Civale, S. Shingubara, P. Leunissen, J. Electrochem. Soc. 159 (7) (2012) D437–D441.
[18] X. Cui, D.A. Hutt, D.J. Scurr, P.P. Conway, J. Electrochem. Soc. 158 (3) (2011) D172.
[19] F. Inoue, T. Shimizu, H. Miyake, R. Arima, T. Ito, H. Seki, Y. Shinozaki, T. Yamamoto, S. Shingubara, Electrochim. Acta 82 (2012) 372–377.
[20] Z. Wang, T. Ida, H. Sakaue, S. Shingubara, T. Takahagi, Electrochem. Solid-State Lett. 6 (3) (2003) C38.